Observationally Constrained Cloud Phase Unmasks Orbitally Driven Climate Feedbacks

N. Sagoo[1,†], T. Storelvmo[1,‡], L. Hahn[1,§], I. Tan[1±], James Danco[2,#], Bryan Raney[2], A.J. Broccoli[2]

[1]Geology & Geophysics Department, Yale University, New Haven, CT 06511, USA

[2]Department of Environmental Sciences, Rutgers, The State University of New Jersey, New Brunswick, NJ 08901, USA

[†]Department of Meteorology, University of Stockholm, 10691 Stockholm, Sweden

[‡]Department of Geosciences, P.O. Box 1047 Blindern, 0316 Oslo, Norway

[§]Department of Atmospheric Sciences, University of Washington, Seattle, WA 98195, USA

[±]NASA Goddard Space Flight Centre, Greenbelt, MD 20771, USA

[#]National Oceanic and Atmospheric Administration, National Weather Service, Raleigh, NC 27606, USA

Corresponding author: Navjit Sagoo and Lily Hahn (navjit.sagoo@misu.su.se, lchahn@uw.edu)

Key Points:

- The cloud phase feedback is weaker in response to orbital forcing when cloud phase is observationally constrained by satellite data
- Cloud and water vapor feedbacks are identified as mechanisms which amplify orbitally driven solar changes and may lead to glaciation
- Improving cloud phase representation in models is important for understanding the climate system response to forcing in the past climates

Abstract

The mechanisms which amplify small orbitally driven changes in insolation and drive the glacial-interglacial cycles of the past 2.7 million years are poorly understood. Previous studies indicate that cloud feedbacks oppose ice sheet initiation at times when orbital configuration supports ice sheet growth. A recent study in which cloud phase was observationally constrained by satellite measurements provides evidence for a weaker opposing cloud feedback than previously found in response to carbon dioxide doubling (Tan et al., 2016). We observationally constrain cloud phase in the Community Earth System Model. We find a weaker cloud phase feedback, which unmasks water vapor and cloud feedbacks that extend cooling to lower latitudes. Snowfall accumulation and ablation metrics also support ice sheet expansion as seen in proxy records. Our results indicate that well understood cloud and water vapor feedbacks are the amplifying mechanism driving orbital climates.

Plain Language Summary

The recent ice ages represent large transitions in climate that are forced by small changes in solar radiation, driven by variations in the Earth's orbit. This study aims to identify the mechanisms that amplify this small solar signal and lead to the development of large ice sheets, as this lack of knowledge indicates gaps in our knowledge of the climate system. Cloud phase (the proportion of liquid to ice) is poorly represented in climate models and previous work has shown that this can lead to an underestimation of the climate response to carbon dioxide forcing. This study explores the climate response to orbital forcing when cloud phase is observationally constrained by satellite. Previous modeling studies have found that when high latitude radiation is reduced due to orbital variations, clouds thin, and allow more solar radiation in, effectively opposing the

orbital cooling that encourages ice sheet growth. We find that when cloud phase is constrained, this opposing cloud thinning is reduced and cooling extends to lower latitudes via cloud and water vapor feedbacks. Our work indicates that well understood climate processes are the mechanisms that amplify orbital climate forcing, and reiterate the importance in properly simulating cloud phase in climate models.

1. Introduction

The Earth has experienced dramatic shifts in climate from glacial to interglacial states during the Pleistocene (the past 2.6 million years), and while these changes are paced by changes in orbital configuration (Hays et al., 1976), there is no satisfactory theory to fully explain how changes in orbit (eccentricity, obliquity and precession) drive ice sheet growth and decay. Milutin Milanković, whose orbital theory is the leading theory today, postulated that changes in Earth's orbit affecting summertime insolation were important in determining global ice volume, and that changes in orbit that led to cooler summers would increase snow and ice preservation (Milanković, 1941). Subsequent work has shown that obliquity is the dominant orbital component recorded in sedimentary archives (Lisiecki & Raymo, 2005; Raymo & Huybers, 2008) and may also be the most important control on integrated summer insolation (P. Huybers, 2006, 2011; P. J. Huybers & Wunsch, 2005). Obliquity has a large impact on seasonality, with low obliquity resulting in cool summers and warm winters, and vice versa for high obliquity.

The mean annual radiative forcing associated with high and low obliquity is much too small to directly drive Pleistocene ice sheet growth and decay. Consequently, large amplifying climate feedbacks are required in order to explain the shifts between glacial and interglacial states with

orbital forcing. Modeling studies which have incorporated orbital changes and additional climate forcings such as CO_2 (Barnola et al., 1987), dust (Lambert et al., 2008), vegetation and topography have had limited success in both simulating glacial inception or glacial melt (Birch et al., 2017; Dong & Valdes, 1995; Jochum et al., 2012, p. 2; Lambert et al., 2008; Rind et al., 1989) and thus the mechanisms behind orbitally driven ice sheet growth and decay are still poorly understood. A study by Erb et al. (2013) quantified the role of radiative feedbacks to changes in obliquity and found that cloud feedbacks impeded ice sheet initiation by opposing glaciation at times when orbital forcing would otherwise support it. A compensating low cloud feedback has also been identified in other studies (Birch et al., 2017; Jochum et al., 2012) providing an additional complication to understanding the orbit-climate relationship. Jochum et al. (2012) first identified a low cloud feedback which opposed orbital forcing from the last glacial inception (115 kya). They calculated that the initial (orbital) forcing of 1.9 Wm^{-2} above 60°N was amplified by the snow-ice-albedo feedback by 6.7 Wm^{-2} and was damped by a negative cloud feedback of 3.1 Wm^{-2}, due to a reduction in low cloud. A later study by Birch et al. (2017) which used a high-resolution cloud resolving model to examine the role of clouds in glacial inception found that CRF became less negative in response to insolation at 115 kya, indicating a negative cloud feedback. Clouds are one of the most challenging and uncertain aspects of the climate system (Boucher et al., 2013) and new research suggest that the negative feedback associated with cloud phase changes in existing models may be too strong (Tan et al., 2016).

Cloud phase is poorly represented in global climate models, which have tended to underestimate the supercooled liquid fraction (SLF) in mixed phase clouds (MPCs) (Cesana et al., 2015;

Komurcu et al., 2014). MPCs are common in the mid and high latitudes (Morrison et al., 2012; Shupe, 2011) but are difficult to model for several reasons: there is a paucity of observational data (Illingworth et al., 2007; Morrison et al., 2012) and general difficulties in representing MPC microphysics (Komurcu et al., 2014; Lohmann & Hoose, 2009), in particular the conversion from liquid to ice known as the Wegner-Bergeron-Findeisen (WBF) process (Storelvmo et al., 2008; Tan & Storelvmo, 2016). The cloud phase feedback can be explained as so: in response to warming the liquid-ice phase transition isotherm moves to higher altitudes such that, for a given altitude, the SLF is enhanced relative to the initial state. For a given amount of cloud water, supercooled liquid droplets are more reflective than cloud ice due to their smaller size and larger population (Murray et al., 2012; Pruppacher & Klett, 1978), thus they are more reflective to shortwave (SW) radiation and oppose the initial warming (Mitchell et al., 1989). When SLFs are initially underestimated, this feedback is too strong and masks other cloud processes that generally yield positive feedbacks (Tan et al., 2016). Using observationally constrained cloud phase, Tan et al. (2016) found that the liquid-to-ice transition isotherm moved upward, where there are fewer and thinner clouds, and poleward where incoming solar radiation is reduced. Subsequently the phase transition response to radiative perturbation is weakened and equilibrium climate sensitivity (ECS) increased.

This study examines the response of observationally constrained modeled clouds to orbital forcing in pairs of simulations in which obliquity is prescribed at the extremes of its Pleistocene range (Lo and Hi simulations). We quantify radiative feedbacks in response to obliquity forcing in two simulations with the Community Earth System Model (CESM) version 1.0.6 in which SLF is constrained to satellite observations (SLF1 and SLF2). This is compared with both a

default (DEF) CESM simulation and corresponding simulations using the GFDL Climate Model, version 2.1 (CM2.1) from Erb et al. (2013).

2. Materials and Methods

2.1. Climate Model Setup

The Community Earth System Model (CESM) version 1.0.6 (Hurrell et al., 2013) is comprised of the atmospheric component CAM5.1 (Liu et al., 2012; Neale et al., 2010) which has 30 vertical levels and uses the three-mode version of the Modal Aerosol Module (MAM3) (Liu et al., 2012); the Community Land Model (CLM4.0) (Lawrence et al., 2011; Oleson et al., 2010); the ocean model (Parallel Ocean Program Ocean model, POP2) (Smith et al., 2010) and the Ice Model (Community Ice CodE, CICE4.0) (Holland et al., 2012; Hunke et al., 2010). In our simulations CAM5.1 and CLM4.0 are run with a resolution of 1.9°x2.5° whilst POP2 and CICE4.0 have a nominal 1° resolution. The DEF simulation is run with the default cloud microphysics scheme (Morrison & Gettelman, 2008) and the standard ice-nucleation parameterization scheme (Meyers et al., 1992) in which ice nucleating particle number concentration is calculated based on temperature and supersaturation. For the SLF1 and SLF2 simulations the ice-nucleation parameterization scheme is updated (DeMott et al., 2015) to a more realistic scheme which enables ice nucleating particle number concentration to be diagnosed as a function of the concentration of large dust particles in addition to temperature. This allows for the spatial and temporal variability of dust IN to be taken into account. As in Tan et al., (2016) SLFs in SLF1 and SLF2 were determined from the results of a 256 member quasi Monte Carlo sampling approach in which six cloud microphysical parameters were modified, and the resulting cloud phase was compared with satellite data from NASA's Cloud-Aerosol-Lidar with Orthogonal Polarization (CALIOP). The parameter combinations selected for

115 SLF1 and SLF2 were very different, but both produced SLFs in excellent agreement with
116 CALIOP.

117 *2.2. Climate Simulations*

118 We use a pre-industrial model configuration (i.e. land mask, ice sheets, greenhouse gases,
119 vegetation and aerosols). Following the methodology of Erb et al. (2013) we perform idealized
120 simulations in which only obliquity is modified to a low (Lo) value of 22.079° and a high (Hi)
121 value of 24.480° representative of the past 600 Kyr. DEF, SLF1 and SLF2 are run with Lo and
122 Hi obliquity (six simulations) for a minimum of 350 years or until the top-of-atmosphere (TOA)
123 energy budget is < 0.3 Wm^{-2}. These simulations are long enough to capture broad changes in
124 the atmosphere and surface ocean but are not long enough for the oceans to fully respond to the
125 obliquity forcing. The final 50 years of the simulation are used as the input for cloud radiative
126 kernel computations, for calculations of climate means and for the International Satellite Cloud
127 Climatology Project (ISCCP) satellite simulator analysis (Klein & Hartmann, 1993; Webb et al.,
128 2001). All results are presented as Lo-Hi anomalies as this convention reduces northern
129 hemisphere (NH) summer insolation, which is conducive to NH glaciation.

130 *2.3. Downscaling Model*

131 As in Notaro et al. (2014), the downscaling employed the SNOW-17 snow accumulation and
132 ablation model (Anderson 2006), which is used by the United States National Weather Service
133 for real-time hydrologic modeling. SNOW-17 is driven by daily temperature and precipitation.
134 Modern snow cover was simulated on a 1° by 1° latitude-longitude grid by using 30 years of
135 observed daily temperature and precipitation from the data set compiled by Kluver et al. (2016).
136 To simulate snow cover in the low obliquity experiments, a simple bias correction approach is
137 used. For each month, climatological differences in surface air temperature were computed

between each low obliquity simulation and a corresponding preindustrial simulation with the same cloud parameterization. These differences were interpolated to the 1° by 1° grid and added to the 30-year observed daily temperature time series at each point. A similar approach was used for precipitation except that the ratio of low obliquity and pre-industrial precipitation was determined, and the observed precipitation time series was multiplied by this ratio.

3. Results

3.1. Temperature and Insolation Seasonal Cycle

Obliquity affects the seasonal cycle of insolation but has a negligible impact on global annual mean insolation, with lower (Lo) obliquity reducing polar insolation in summer and increasing it in winter. Figure 1 shows the annual mean Lo-Hi surface air temperature (SAT) anomaly (colored contours) with the insolation anomaly overlaid (black contours). The negative insolation anomaly (in all simulations) extends across almost all the northern hemisphere (NH) from March to September. In the DEF experiment, negative SAT anomalies lag the insolation anomaly by ~ 6 weeks and have a smaller spatial and temporal extent than the negative anomalies in SLF1 and SLF2. In SLF1 and SLF2 negative SAT anomalies extend equator-wards in March and over the entire NH (and globe) until January where a very small 0.25 K tropical warming occurs.

Negative SAT anomalies in SLF1 and SLF2 extend into areas with a positive insolation anomaly and indicate the importance of climate feedbacks over local radiative balance. The Lo-Hi global annual mean SAT anomalies for our experiments are -0.79 K, -1.30 K and -1.36 K for DEF, SLF1 and SLF2 respectively, while in CM2.1 the Lo-Hi anomaly is 0.5 K. These SAT anomalies indicate that the climate response to obliquity forcing is considerably larger when cloud phase is observationally constrained.

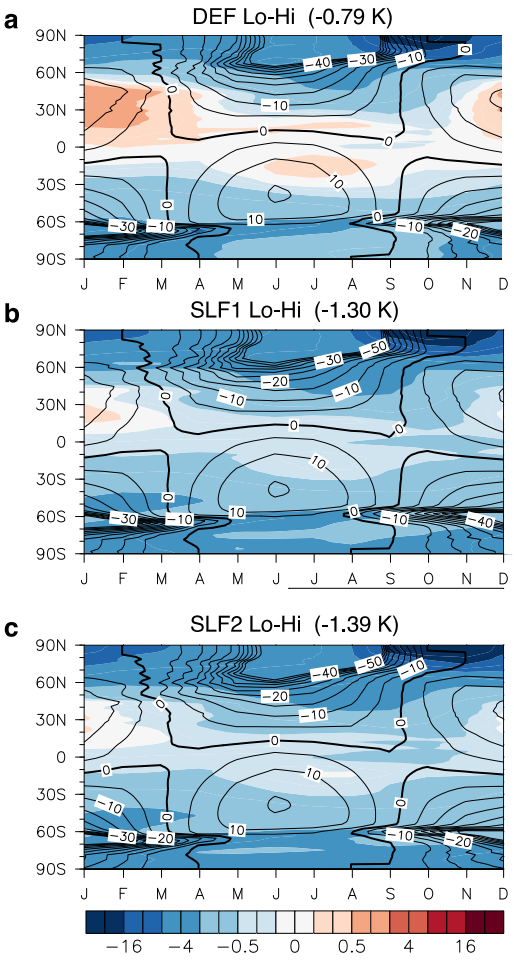

Figure 1. Seasonal changes in surface air temperature (SAT) and insolation shown as Lo-Hi obliquity anomalies. a) DEF, b) SLF1 and c) SLF2. SAT is shown in colored contours with the global annual mean SAT anomaly value shown at the top of each figure in parenthesis. Overlaid black contours and labels denote the Lo-Hi insolation anomaly with the thick black line indicating the zero-insolation contour.

3.2. Radiative Feedbacks

We calculate the radiative feedbacks of surface albedo, atmospheric water vapor, vertical temperature lapse rate and cloud optical properties using the radiative kernel method of climate feedback analysis (Shell et al., 2008; Soden et al., 2008). Note that results are presented as the effect of feedbacks on net TOA radiation ΔR_{net} (Wm^{-2}) and not as feedbacks ($Wm^{-2}\,K^{-1}$). A positive value thus indicates a warming (damping) feedback while a negative value indicates a

cooling (amplifying) feedback. Globally, the total feedback is ~1.6 to 1.7 times stronger in SLF1 and SLF2 compared to DEF (Figure 2a) and 2.2 to 2.4 times stronger than that found in CM2.1. Both the cloud and water vapor feedbacks are much larger in SLF1 and SLF2 compared to DEF and CM2.1, whilst the lapse rate feedback is similar in all simulations and the surface albedo feedback is only marginally larger in SLF1 and SLF2. When broken down into regions (Figure 2b-d) the mid-latitude cloud feedback and tropical water vapor feedback stand out as being much larger in SLF1 and SLF2 compared to DEF.

During late summer in the high latitudes low obliquity conditions reduce insolation in this region, which should result in local cooling. Over this period in DEF, column-integrated liquid (liquid water path, LWP) reduces and acts to oppose and reduce cooling from this obliquity driven reduction in insolation (Figure S1). This process is also seen in CM2.1. In the SLF1 and SLF2 simulations this high-latitude LWP reduction in summer is not evident, but a large increase in total (ice+liquid) water path (TWP) appears in the mid-latitudes (30-60°N) which increases cloud reflectivity and thus cooling throughout the year (Figure S1).

In response to obliquity forcing (Lo-Hi), cooling leads to cloud liquid being converted to cloud ice, which is optically thinner. The cloud phase bias in DEF causes an exaggerated cloud thinning as too much liquid is converted to ice with cooling. This exaggerated reduction in cloud optical depth counters the other, mainly positive, cloud feedbacks and therefore weakens the spreading of high-latitude cooling to mid- and low latitudes. In contrast, the amplifying mid-latitude cloud feedback in SLF1 and SLF2 is twice as strong as in DEF, permitting high-latitude cooling to spread across the mid-latitudes towards the tropics. The slight cooling in the tropics (as opposed to the warming seen in DEF and CM2.1) is accompanied by a slight decrease in atmospheric water vapor, as expected according to the Clausius-Clapeyron relation. Since water

197 vapor is a potent greenhouse gas, this reduction in water vapor increases outgoing longwave
198 (LW) radiation and thus constitutes a powerful amplifying feedback in the tropics. The negative
199 (amplifying) water vapor feedback is enabled by the strong mid-latitude cloud feedback, because
200 in its absence the summer Lo-Hi insolation anomaly in the tropics, which is slightly positive,
201 would produce a warming and thus a positive water vapor feedback that would act to oppose to
202 the orbital forcing (as seen in DEF and in CM2.1).

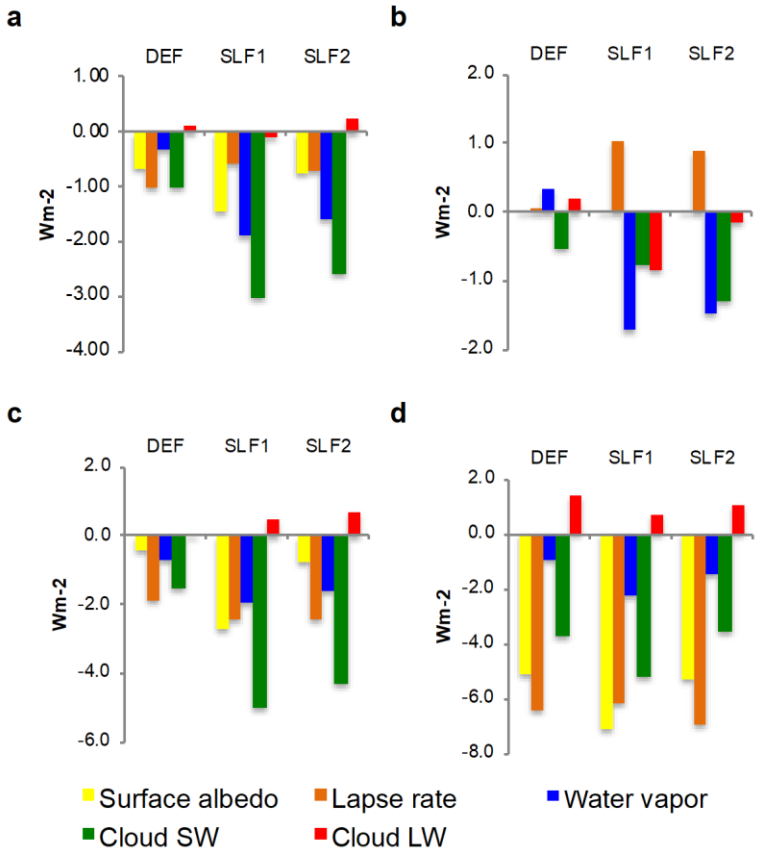

203

204 **Figure 2**. Radiative feedbacks are partitioned into individual components (surface albedo, lapse
205 rate, water vapor, cloud shortwave (SW), cloud longwave (LW) and presented for different
206 regions. a) Global mean; b) low-latitudes (20°S-20°N; c) mid-latitudes (30-60°N and S) and d)
207 high latitudes (60-90°N and S). Results are presented as the effect of feedbacks on net TOA
208 radiation (Wm^{-2}) and not as surface temperature-mediated feedbacks (Wm^{-2} K^{-1}).

3.3. Decomposing the Cloud (Feedback) Response to Orbital Forcing

In order to more fully understand the changes in cloud properties that occur in response to orbital forcing we examine the output from the International Satellite Cloud Climatology Project satellite simulator (ISCCP) (Klein & Jakob, 1999; Webb et al., 2001) which is implemented in the atmosphere component of CESM, the Community Atmosphere Model (CAM5.1). The ISCCP simulator allows cloud properties in models to be diagnosed in a manner consistent with the satellite view from space. The radiative impact of changes in cloud amount (CLD), optical depth (COT) and cloud top pressure (CTP) as well as a residual term are calculated following Zelinka et al. (2012) and summarized by feedback in Figure 3 with the net feedback shown in Figure S2. This de-composition of the net (SW+LW) cloud feedback into contributions from CLD, CTP and COT reveals that the latter component is responsible for the difference in mid-latitude cloud feedback between DEF on one hand, and SLF1 and SLF2 on the other. Because the orbital signal is strongest in 60-90°N, it helps to consider this region first. In DEF COT is positive whilst in SLF1 and SLF2 it has shifted to less positive values. Now if we consider 60-90°N, COT has decreased from near zero in DEF, to up to -3 Wm^{-2} in SLF1 and SLF2 across this latitude band. This is consistent with the expectation that cloud thinning associated with cloud phase changes should be substantially weakened in the simulations with observationally-constrained SLF.

3.4. Glacial inception

The central tenet of Milanković' orbital theory is that cooler summers allow high latitude snow to survive the summer melt season. Perennial snow cover subsequently leads to snow-albedo feedbacks, which amplify ice cap expansion and initiate the growth of large-scale ice-sheets. Sediment cores indicate that in the NH the last glacial inception occurred ~ 115,000 years ago in

the region of Hudson Bay and Baffin Island over a period of around 20,000 years (Clark et al., 1993). We gauge the summer melt response to the cooling signal in these experiments by calculating the percentage change in positive degree-days (PDD) for the June-July-August (JJA) period (Figure 4a-c). All three experiments show a substantial reduction in PDD (up to 50%) in the high Arctic, Hudson Bay area and over Baffin Island, which are likely locations of the last initiation of the Laurentide ice sheet. In SLF1 and SLF2 the reduction in PDD extends further into the mid-latitudes than DEF, in agreement with the increased extent of negative SATs.

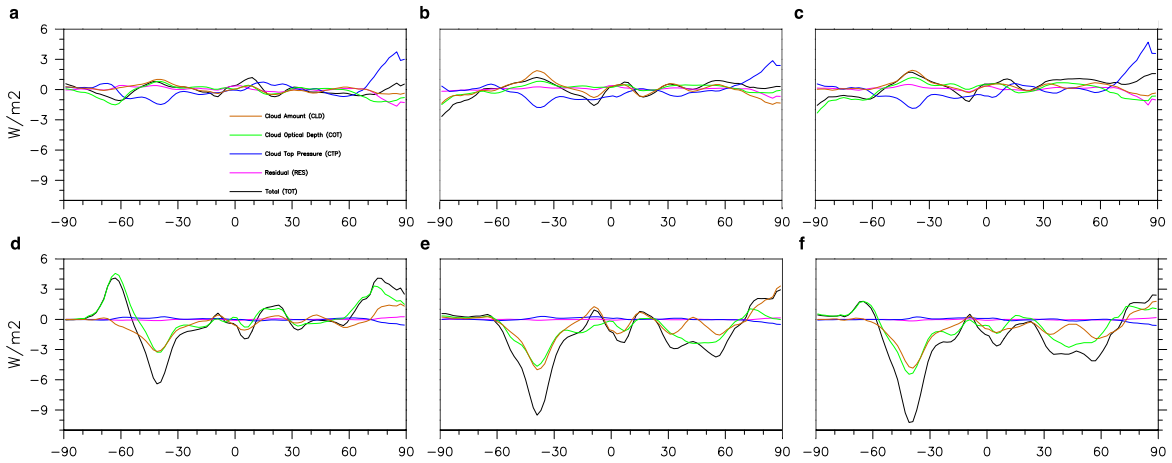

Figure 3. Longwave (LW) and shortwave (SW) cloud feedbacks calculated using the International Satellite Cloud Climatology Project satellite simulator (ISCCP). LW feedbacks are shown in the top row: a) DEF, b) SLF1, c) SLF2, SW feedbacks are shown in the bottom row: d) DEF, e) SLF1 and f) SLF2 with feedbacks due to changes in cloud amount (CLD) shown in orange, cloud optical depth (COT) in green, cloud top pressure (CTP) in blue, a residual component in magenta and total feedbacks are shown in black.

Because climate model resolutions are too coarse to capture the detail required for realistic ice sheet dynamics (i.e. underlying bedrock topography) (Pollard & Thompson, 1997), a downscaling approach was also used to determine the extent to which the differences in cloud parametrization would affect the persistence of snow cover in the low obliquity simulations (see methods). Figure 4d-e shows the average number of days without snow cover > 1" for the Lo-

Preindustrial anomaly over the Canadian Arctic. SLF1 and SLF2 have fewer snow free days over the summer than DEF, with this increase in snow preservation occurring over the southern part of Baffin Island, eastwards of the Hudson Bay and over much of northern and middle Canada, which is in line with the proxy evidence. Because modern simulations were not available for this study, and the modern climate is warmer than the preindustrial climate, our use of pre-industrial anomalies likely underestimates the duration of snow cover in the low obliquity experiments.

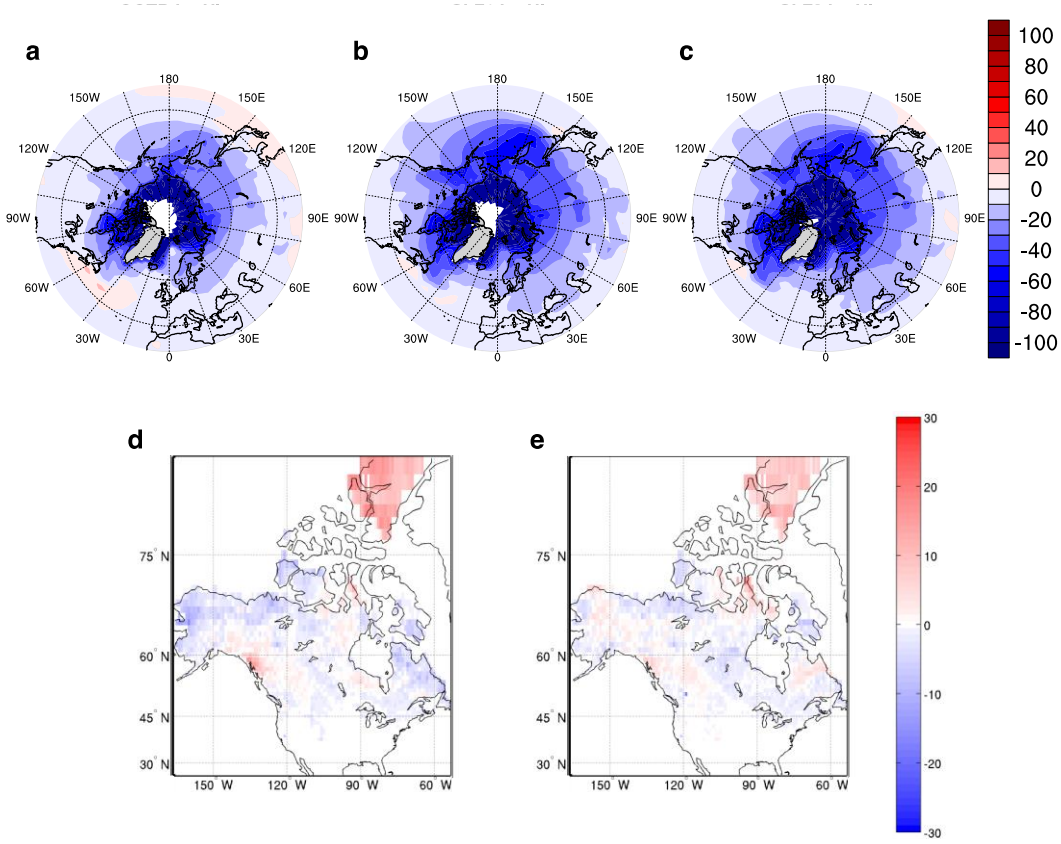

Figure 4. Indicators of change in summer (June, July, August) snow preservation. Percentage change in positive-degree days (PDD) polewards of 30°N for northern hemisphere for Lo-Hi anomaly shown for a) DEF, b) SLF1 and c) SLF2 Lo-Hi experiments with blue indicating fewer PDD and increased likelihood of snow preservation. A downscaling model was used to calculate the average number of days without snow $\geq$ 1" in the Canadian Arctic for the Lo-Pre-industrial anomaly for DEF, SLF1 and SLF2. The anomaly of d) SLF1-DEF and e) SLF2-DEF are shown in the bottom row where blue indicates an increase in snow covered days.

4. Discussion and Conclusions

We have repeated the experiments in Erb et al. (2013) to examine the obliquity driven climate response in a model with observationally constrained supercooled liquid fraction (SLF) in mixed phase clouds (MPCs). SLFs are increased in two experiments (SLF1 and SLF2) using a more realistic ice-nucleation scheme (DeMott et al., 2015) but using different methods in order to account for the uncertainties associated with MPC microphysics. These are compared with a default model (DEF) in which SLFs are known to be underestimated (Cesana et al., 2015; Komurcu et al., 2014). Other studies have found that orbitally induced climate changes are opposed by reductions in high latitude low level cloud (Birch et al., 2017; Erb et al., 2013; Jochum et al., 2012). However, when realistic SLFs are used, this negative cloud feedback is reduced which allows obliquity-driven cooling to spread to lower latitudes. This cooling leads to an increased liquid water path (LWP) and ice water path (IWP) in mid-latitude clouds and this positive cloud feedback further extends the cooling signal both throughout the year and leads to a strong tropical water vapor feedback. Overall the SAT response in SLF1 and SLF2 is 2-3 times larger than that in CM2.1 whilst the sum of radiative feedbacks are 1.6 - 2.3 times larger in SLF1 and SLF2 compared with DEF and CM2.1. Reductions in positive degree days (PDDs) of up to 50% occur in the summer melt season in the Hudson Bay and Baffin Island area which have been identified as probable locations for the expansion of the Laurentide ice sheet (Clark et al., 1993). These and further reductions in PDD which extend into the mid-latitudes in SLF1 and SLF2, and reduction in snow-free days calculated from the downscaling approach provide further support that the climate in these experiments is more conducive to ice-sheet growth. The processes that contribute to the extension and expansion of the cooling signal are the same in

both hemispheres unlike other studies in which only a strong northern hemisphere signal is simulated (Jochum et al., 2012).

Simulating cloud processes is a challenging area of study and it should be noted that the microphysics that contribute to high SLFs in mixed phase clouds are not completely understood: both reductions in the efficiency of the Wegner-Bergeron-Findeisen (WBF) process (Lohmann & Hoose, 2009; Storelvmo et al., 2008; Tan & Storelvmo, 2016) and the availability, size distribution and effectiveness of ice nucleating particles such as mineral dust (Atkinson et al., 2013; Kok et al., 2017; Murray et al., 2012; Sagoo & Storelvmo, 2017) have a significant impact on SLFs and climate. The positive feedbacks which amplify the orbital signal in this work were only unmasked because the high latitude negative cloud feedback was not present in SLF1 and SLF2. Understanding the response of low Arctic clouds to changes in climate and sea-ice cover is challenging (Kay et al., 2011; Kay & Gettelman, 2009) and thus the magnitude and even the presence of a high latitude summer low cloud feedback are still not well constrained. Finally, in summary, we find strong support for Milanković's orbital theory in this study when SLFs are observationally constrained. Enhanced cooling in the high latitudes leads to the unmasking of well-known positive mid-latitude cloud feedbacks and tropical water vapor feedback, which amplify the obliquity signal by additional cooling which reduces summer snow/ice melt.

Acknowledgments, Samples, and Data

- Simulations were run on the Yale High Performance Computing Cluster.
- CESM model output for this study is available at http://doi.org/10.5281/zenodo.3891912.
- The authors declare no competing interests.

Author contributions

A.B conceived the project, A.B, T.S and N.S designed and organized this study. L.H, N.S, T.S, A.B carried out the analysis. J.D and B.R developed the downscaling software and made the calculations. L.H, N.S and T.S wrote the manuscript. All authors discussed and contributed to the manuscript.

References

Atkinson, J. D., Murray, B. J., Woodhouse, M. T., Whale, T. F., Baustian, K. J., Carslaw, K. S., et al. (2013). The importance of feldspar for ice nucleation by mineral dust in mixed-phase clouds. *Nature*, *498*(7454), 355–358.

Barnola, J.-M., Raynaud, D., Korotkevich, Y. S., & Lorius, C. (1987). Vostok ice core provides 160,000-year record of atmospheric CO2. *Nature*, *329*(6138), 408–414.

Birch, L., Cronin, T., & Tziperman, E. (2017). Glacial Inception on Baffin Island: The Role of Insolation, Meteorology, and Topography. *Journal of Climate*, *30*(11), 4047–4064. https://doi.org/10.1175/JCLI-D-16-0576.1

Boucher, O., Randall, D., Artaxo, P., Bretherton, C., Feingold, G., Forster, P., et al. (2013). Clouds and Aerosols: In Climate Change 2013: The Physical Science Basis Contribution of Working Group I to the Fifth Assessment Report of the Intergovernmental Panel on Climate Change. *K., Tignor, M., Allen, SK, Boschung, J., Nauels, A., Xia, Y., Bex, V., Midgley, PM, Eds*.

Cesana, G., Waliser, D. E., Jiang, X., & Li, J.-L. (2015). Multimodel evaluation of cloud phase transition using satellite and reanalysis data. *Journal of Geophysical Research: Atmospheres*, *120*(15), 7871–7892.

Clark, P. U., Clague, J. J., Curry, B. B., Dreimanis, A., Hicock, S. R., Miller, G. H., et al. (1993). Initiation and development of the Laurentide and Cordilleran ice sheets following the last interglaciation. *Quaternary Science Reviews*, *12*(2), 79–114.

DeMott, P. J., Prenni, A. J., McMeeking, G. R., Sullivan, R. C., Petters, M. D., Tobo, Y., et al. (2015). Integrating laboratory and field data to quantify the immersion freezing ice nucleation activity of mineral dust particles. *Atmospheric Chemistry and Physics*, *15*(1), 393–409.

339 Dong, B., & Valdes, P. J. (1995). Sensitivity studies of Northern Hemisphere glaciation using an
340 atmospheric general circulation model. *Journal of Climate*, *8*(10), 2471–2496.
341 Erb, M. P., Broccoli, A. J., & Clement, A. C. (2013). The contribution of radiative feedbacks to
342 orbitally driven climate change. *Journal of Climate*, *26*(16), 5897–5914.
343 Hays, J. D., Imbrie, J., Shackleton, N. J., & others. (1976). Variations in the Earth's orbit:
344 pacemaker of the ice ages. American Association for the Advancement of Science.
345 Retrieved from
346 https://www.researchgate.net/profile/J_Hays/publication/301325552_Variations_in_the_
347 Earth_pacemaker_of_the_ice_ages/links/573cca0c08ae9ace840fe240.pdf
348 Holland, M. M., Bailey, D. A., Briegleb, B. P., Light, B., & Hunke, E. (2012). Improved sea ice
349 shortwave radiation physics in CCSM4: the impact of melt ponds and aerosols on Arctic
350 sea ice*. *Journal of Climate*, *25*(5), 1413–1430.
351 Hunke, E. C., Lipscomb, W. H., Turner, A. K., & others. (2010). CICE: the Los Alamos Sea Ice
352 Model Documentation and Software User's Manual Version 4.1 LA-CC-06-012. *T-3*
353 *Fluid Dynamics Group, Los Alamos National Laboratory*, *675*. Retrieved from
354 http://oceans11.lanl.gov/svn/CICE/tags/release-5.1/doc/cicedoc.pdf
355 Hurrell, J. W., Holland, M. M., Gent, P. R., Ghan, S., Kay, J. E., Kushner, P. J., et al. (2013).
356 The community earth system model: a framework for collaborative research. *Bulletin of*
357 *the American Meteorological Society*, *94*(9), 1339–1360.
358 Huybers, P. (2006). Early Pleistocene glacial cycles and the integrated summer insolation
359 forcing. *Science*, *313*(5786), 508–511.
360 Huybers, P. (2011). Combined obliquity and precession pacing of late Pleistocene deglaciations.
361 *Nature*, *480*(7376), 229–232.

Huybers, P. J., & Wunsch, C. (2005). Obliquity pacing of the late Pleistocene glacial terminations. Retrieved from https://dash.harvard.edu/handle/1/3382978

Illingworth, A. J., Hogan, R. J., O'connor, E. J., Bouniol, D., Delanoë, J., Pelon, J., et al. (2007). Cloudnet: Continuous evaluation of cloud profiles in seven operational models using ground-based observations. *Bulletin of the American Meteorological Society*, *88*(6), 883–898.

Jochum, M., Jahn, A., Peacock, S., Bailey, D. A., Fasullo, J. T., Kay, J., et al. (2012). True to Milankovitch: Glacial inception in the new community climate system model. *Journal of Climate*, *25*(7), 2226–2239.

Kay, J. E., & Gettelman, A. (2009). Cloud influence on and response to seasonal Arctic sea ice loss. *Journal of Geophysical Research: Atmospheres*, *114*(D18), D18204. https://doi.org/10.1029/2009JD011773

Kay, J. E., Holland, M. M., & Jahn, A. (2011). Inter-annual to multi-decadal Arctic sea ice extent trends in a warming world. *Geophysical Research Letters*, *38*(15), L15708. https://doi.org/10.1029/2011GL048008

Klein, S. A., & Hartmann, D. L. (1993). The Seasonal Cycle of Low Stratiform Clouds. *Journal of Climate*, *6*(8), 1587–1606. https://doi.org/10.1175/1520-0442(1993)006<1587:TSCOLS>2.0.CO;2

Klein, S. A., & Jakob, C. (1999). Validation and sensitivities of frontal clouds simulated by the ECMWF model. *Monthly Weather Review*, *127*(10), 2514–2531.

Kluver, D., Mote, T., Leathers, D., Henderson, G. R., Chan, W., & Robinson, D. A. (2016). Creation and validation of a comprehensive 1 by 1 daily gridded North American dataset

for 1900–2009: Snowfall. *Journal of Atmospheric and Oceanic Technology*, *33*(5), 857–871.

Kok, J. F., Ridley, D. A., Zhou, Q., Miller, R. L., Zhao, C., Heald, C. L., et al. (2017). Smaller desert dust cooling effect estimated from analysis of dust size and abundance. *Nature Geoscience*, *10*(4), 274–278. https://doi.org/10.1038/ngeo2912

Komurcu, M., Storelvmo, T., Tan, I., Lohmann, U., Yun, Y., Penner, J. E., et al. (2014). Intercomparison of the cloud water phase among global climate models. *Journal of Geophysical Research: Atmospheres*, *119*(6), 2013JD021119. https://doi.org/10.1002/2013JD021119

Lambert, F., Delmonte, B., Petit, J.-R., Bigler, M., Kaufmann, P. R., Hutterli, M. A., et al. (2008). Dust-climate couplings over the past 800,000 years from the EPICA Dome C ice core. *Nature*, *452*(7187), 616–619.

Lawrence, D. M., Oleson, K. W., Flanner, M. G., Thornton, P. E., Swenson, S. C., Lawrence, P. J., et al. (2011). Parameterization improvements and functional and structural advances in Version 4 of the Community Land Model. *Journal of Advances in Modeling Earth Systems*, *3*(1), M03001. https://doi.org/10.1029/2011MS00045

Lisiecki, L. E., & Raymo, M. E. (2005). A Pliocene-Pleistocene stack of 57 globally distributed benthic δ18O records. *Paleoceanography*, *20*(1). Retrieved from http://onlinelibrary.wiley.com/doi/10.1029/2004PA001071/full

Liu, X., Easter, R. C., Ghan, S. J., Zaveri, R., Rasch, P., Shi, X., et al. (2012). Toward a minimal representation of aerosols in climate models: Description and evaluation in the Community Atmosphere Model CAM5. *Geoscientific Model Development*, *5*(3), 709.

406 Lohmann, U., & Hoose, C. (2009). Sensitivity studies of different aerosol indirect effects in
407 mixed-phase clouds. *Atmospheric Chemistry and Physics*, *9*(22), 8917–8934.
408 Meyers, M. P., DeMott, P. J., & Cotton, W. R. (1992). New primary ice-nucleation
409 parameterizations in an explicit cloud model. *Journal of Applied Meteorology*, *31*(7),
410 708–721.
411 Milanković, M. (1941). *Kanon der Erdbestrahlung und seine Anwendung auf das*
412 *Eiszeitenproblem*. na.
413 Mitchell, J. F., Senior, C. A., & Ingram, W. J. (1989). C02 and climate: a missing feedback?
414 *Nature*, *341*(6238), 132–134.
415 Morrison, H., & Gettelman, A. (2008). A New Two-Moment Bulk Stratiform Cloud
416 Microphysics Scheme in the Community Atmosphere Model, Version 3 (CAM3). Part I:
417 Description and Numerical Tests. *Journal of Climate*, *21*(15), 3642–3659.
418 https://doi.org/10.1175/2008JCLI2105.1
419 Morrison, H., de Boer, G., Feingold, G., Harrington, J., Shupe, M. D., & Sulia, K. (2012).
420 Resilience of persistent Arctic mixed-phase clouds. *Nature Geoscience*, *5*(1), 11–17.
421 https://doi.org/10.1038/ngeo1332
422 Murray, B. J., O'Sullivan, D., Atkinson, J. D., & Webb, M. E. (2012). Ice nucleation by particles
423 immersed in supercooled cloud droplets. *Chemical Society Reviews*, *41*(19), 6519–6554.
424 Neale, R. B., Chen, C.-C., Gettelman, A., Lauritzen, P. H., Park, S., Williamson, D. L., et al.
425 (2010). Description of the NCAR community atmosphere model (CAM 5.0). *NCAR*
426 *Tech. Note NCAR/TN-486+ STR*. Retrieved from
427 https://www.ccsm.ucar.edu/models/ccsm4.0/cam/docs/description/cam4_desc.pdf

Notaro, M., Lorenz, D., Hoving, C., & Schummer, M. (2014). Twenty-first-century projections of snowfall and winter severity across central-eastern North America. *Journal of Climate*, *27*(17), 6526–6550.

Oleson, K. W., Lawrence, D. M., Gordon, B., Flanner, M. G., Kluzek, E., Peter, J., et al. (2010). Technical description of version 4.0 of the Community Land Model (CLM). Retrieved from http://citeseerx.ist.psu.edu/viewdoc/summary?doi=10.1.1.172.7769

Pollard, D., & Thompson, S. L. (1997). Driving a high-resolution dynamic ice-sheet model with GCM climate: ice-sheet initiation at 116 000 BP. *Annals of Glaciology*, *25*, 296–304.

Pruppacher, H. R., & Klett, J. D. (1978). Microphysics ofclouds andprecipitation. *Reidel, Dordrecht, Holland, 714pp*.

Raymo, M. E., & Huybers, P. (2008). Unlocking the mysteries of the ice ages. *Nature*, *451*(7176), 284–285.

Rind, D., Peteet, D., & Kukla, G. (1989). Can Milankovitch orbital variations initiate the growth of ice sheets in a general circulation model? *Journal of Geophysical Research: Atmospheres*, *94*(D10), 12851–12871.

Sagoo, N., & Storelvmo, T. (2017). Testing the sensitivity of past climates to the indirect effects of dust. *Geophysical Research Letters*, *44*(11), 2017GL072584. https://doi.org/10.1002/2017GL072584

Shell, K. M., Kiehl, J. T., & Shields, C. A. (2008). Using the radiative kernel technique to calculate climate feedbacks in NCAR's Community Atmospheric Model. *Journal of Climate*, *21*(10), 2269–2282.

Shupe, M. D. (2011). Clouds at Arctic atmospheric observatories. Part II: Thermodynamic phase characteristics. *Journal of Applied Meteorology and Climatology*, *50*(3), 645–661.

Smith, R., Jones, P., Briegleb, B., Bryan, F., Danabasoglu, G., Dennis, J., et al. (2010). The parallel ocean program (POP) reference manual ocean component of the community climate system model (CCSM) and community earth system model (CESM). *Rep. LAUR-01853*, *141*, 1–140.

Soden, B. J., Held, I. M., Colman, R., Shell, K. M., Kiehl, J. T., & Shields, C. A. (2008). Quantifying climate feedbacks using radiative kernels. *Journal of Climate*, *21*(14), 3504–3520.

Storelvmo, T., Kristjánsson, J. E., Lohmann, U., Iversen, T., Kirkev\a ag, A., & Seland, Ø. (2008). Modeling of the Wegener–Bergeron–Findeisen process—implications for aerosol indirect effects. *Environmental Research Letters*, *3*(4), 045001.

Tan, I., & Storelvmo, T. (2016). Sensitivity study on the influence of cloud microphysical parameters on mixed-phase cloud thermodynamic phase partitioning in CAM5. *Journal of the Atmospheric Sciences*, *73*(2), 709–728.

Tan, I., Storelvmo, T., & Zelinka, M. D. (2016). Observational constraints on mixed-phase clouds imply higher climate sensitivity. *Science*, *352*(6282), 224–227.

Webb, M., Senior, C., Bony, S., & Morcrette, J.-J. (2001). Combining ERBE and ISCCP data to assess clouds in the Hadley Centre, ECMWF and LMD atmospheric climate models. *Climate Dynamics*, *17*(12), 905–922.

Zelinka, M. D., Klein, S. A., & Hartmann, D. L. (2012). Computing and partitioning cloud feedbacks using cloud property histograms. Part I: Cloud radiative kernels. *Journal of Climate*, *25*(11), 3715–3735.